A Recharging Mechanism for Improving Data Quality and Maintaining Sustainable Lifetime in WRSNs

Zhijie Hu, Chih-Yung Chang, *Member, IEEE*, Ruibing Shen, Chin-Hwa Kuo, and Diptendu Sinha Roy

***Abstract*—The wireless recharging technology of wireless sensor networks (WSNs) has received much attention in recent years. In literature, many studies assumed that the sensors are static and aimed to increase the number of recharged sensors and reduce the traveling path of the mobile charger. Since the given WSNs consisted of a large number of sensors that were usually deployed in a wide monitoring region, it is time-consuming for the mobile charger to visit all sensors and recharge them. This article considers the mobile wireless rechargeable sensor networks (MWRSNs) where all sensors are assumed to be mobile, and hence, they can adopt mobility to reduce the overhead of the mobile charger in terms of traveling cost. The proposed recharging mechanism initially determines the number and the locations of recharging stations. Then, the proposed algorithm further exploits the cooperation opportunities between the sensors and the mobile charger to improve recharging efficiency and data quality. In addition, the proposed algorithm further finds the bottleneck location, which has the lowest data quality and then relocates the sensors according to their workloads, aiming to maximize the data quality by breaking the bottleneck. The experimental results reveal that the proposed algorithm outperforms the related studies in terms of recharging efficiency and data quality.**

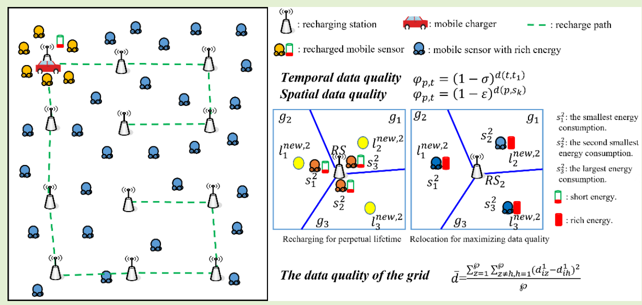

***Index Terms*—Mobile sensors, spatial data quality, temporal data quality, wireless sensor network (WSN).**

NOMENCLATURE

L	Length and width of the monitoring region.
W	Width and width of the monitoring region.
S	Set of n sensors deployed in the monitoring region, $S = \{s_1, s_2, \ldots, s_n\}$.
e_M^{char}	Recharging rate of the mobile charger.
$e_M^{\text{move\_disch}}$	Moving discharging rate of the mobile charger.
v_M	Moving speed of the mobile charger.
E_{charger}	Battery capacity of the mobile charger.
E_{sensor}	Battery capacity of each sensor.
v_s	Moving speed of each mobile sensor.
$e_s^{\text{move\_disch}}$	Moving discharging rate of the sensor.
$e_k^{\text{work\_disch}}$	Energy discharging rate of the sensor s_k for working.
f_k	Sensing frequency of the sensor s_k.
$\varphi_{p,t}^{\text{temporal}}$	Temporal data quality of point p at time t.
$\varphi_{p,t}^{\text{spatial}}$	Spatial data quality of point p at time t.
$\varphi_{p,t}$	Data quality of point p at time t.
σ	Loss rate of data quality per unit time.
ε	Loss rate of data quality per unit distance.
Q	Data quality of the whole monitoring region in period T.
m	Number of the subregions.
R_i^{sub}	ith subregion.
RS_i	Center point of the subregion R_i^{sub}.
S_i	Set of sensors located in subregion R_i^{sub}, $S_i = \{s_1^i, s_2^i, \ldots, s_{\lvert S_i\rvert}^i\}$.
$l_k^{\text{old},i}$	Original location of the sensor $s_k^i \in S_i$ in subregion R_i^{sub}.

Manuscript received 29 January 2023; accepted 21 September 2023. Date of publication 9 October 2023; date of current version 14 November 2023. This work was supported in part by the University-Level Key Course Project "Smart Hardware" under Project 2019KC002, in part by the Special Scientific Research Plan of Education Department of Shaanxi Provincial Government under Project 21JK0817, and in part by the Shaanxi Provincial Department of Science and Technology Key Research and Development Program under Project 2022GY-317. The associate editor coordinating the review of this article and approving it for publication was Dr. Thilo Sauter. *(Corresponding author: Chin-Hwa Kuo.)*

Zhijie Hu is with Xi'an Jiaotong University, Xi'an 710000, China, and also with the School of Information Engineering, Xi'an Eurasia University, Xi'an 710000, China (e-mail: huzhijie@eurasia.edu).

Chih-Yung Chang and Chin-Hwa Kuo are with the Department of Computer Science and Information Engineering, Tamkang University, New Taipei 25137, Taiwan (e-mail: cychang@mail.tku.edu.tw; chinhwakuo@mail.tku.edu.tw).

Ruibing Shen is with the School of Information Engineering, Xi'an Eurasia University, Xi'an 710000, China (e-mail: shenruibing@eurasia.edu).

Diptendu Sinha Roy is with the Department of Computer Science and Engineering, National Institute of Technology Meghalaya, Shillong 793003, India (e-mail: diptendu.sr@nitm.ac.in).

Digital Object Identifier 10.1109/JSEN.2023.3321330

$l_k^{\text{new},i}$ Relocated location of the sensor $s_k^i \in S_i$ in sub-region R_i^{sub}.
$T_k^{\text{ford},i}$ Time required for the sensor $s_k^i \in S_i$ moving from $l_k^{\text{old},i}$ to the recharging station RS_i.
$E_k^{\text{ford},i}$ Energy required for the sensor $s_k^i \in S_i$ moving from $l_k^{\text{old},i}$ to the recharging station RS_i.
$T_k^{\text{back},i}$ Time required for the sensor $s_k^i \in S_i$ moving from the recharging station RS_i to the relocated location $l_k^{\text{new},i}$.
$E_k^{\text{back},i}$ Energy required for the sensor $s_k^i \in S_i$ moving from the recharging station RS_i to the relocated location $l_k^{\text{new},i}$.

I. Introduction

Wireless sensor networks (WSNs) are self-organizing networks consisting of many sensor nodes [1]. WSNs have been widely used to support various monitoring and control applications, such as environmental surveillance, industrial sensing, disaster management, military applications, traffic checking, and so on [2], [3], [4], [5]. However, each sensor is battery-powered [6], which leads to a limited lifetime and constrains the applications of WSNs.

To cope with the limited lifetime problem, many researchers have devoted their efforts to sustaining the lifetime of WSNs in recent years. These studies fall into two categories: energy harvesting technology and wireless charging technology. The energy harvesting technology can convert natural energy, such as wind energy, solar energy, geothermal energy, and vibration energy, into electrical energy to support the energy required for sensors in the WSN [7], [8], [9]. However, the energy source of this technology was not stable. On the other hand, wireless charging technology usually adopts the mobile charger to charge sensors [10], [11]. The mobile charger received the recharging requests from sensors and constructed the recharging path along which the requested sensors can be recharged.

In the class of wireless charging technology, many studies have been proposed.

These studies can be further classified into two categories: offline and online schedules. In the category of offline schedule, the mobile charger received the recharging requests from sensors and then made a recharge schedule. According to the schedule, the mobile charger constructed a recharge path along which it moves to the sensor and recharges the sensor until it finished the recharging task. Then, the mobile charger further considered the other requests. The offline schedule guaranteed that the sensors that have been already scheduled in the recharging path can be recharged without occurring the starvation problem. However, as soon as the recharging schedule has been made, the mobile charger did not consider the other new recharging requests sent from the other sensors, resulting in low recharging efficiency due to the long recharging path and the lack of flexibility.

To improve the disadvantages of the offline schedule, the online schedule that timely considered the new request and dynamically reconstructed the recharging path can achieve better recharging efficiency. This occurs because the newly requested sensors might be inserted in the newly constructed path if their locations were close to the constructed path. However, the mobile charger still needed to move to each scheduled sensor along the constructed path and then recharge it. The moving and recharging operations were time-consuming. As a result, many sensors were unable to be recharged, and hence, they were finally energy exhausted, leading to low surveillance quality of the monitoring region.

Some other studies [12], [13], [14] considered the mobile WSNs (MWSNs) where all or part of the sensors were mobile. In the MWSNs, the mobility of sensors helps reduce the workload of the mobile charger since they can move to specific locations and wait for obtaining energy from the mobile charger. Though the workload of the mobile charger can be reduced, it still needs more effort to improve the data quality since the cooperation between mobile sensors and the mobile charger is important and can impact the performance in terms of data quality.

This article considers the MWSNs and develops a recharging mechanism that exploits the cooperation opportunities between mobile sensors and the mobile charger, aiming at maximizing the data quality. The proposed recharging mechanism not only considers the recharging efficiency and recharging cost but also considers the data quality, including spatial data quality and temporal data quality.

The main contributions of the proposed algorithm are itemized as follows.

A. Maximizing Data Quality

This article considers not only spatial data quality but also temporal data quality, aiming to maximize the data quality of the monitoring area. The proposed algorithm considers the spatial and temporal data qualities that are different from the related work [18], [19], [20], [21], [22].

In most related work [18], [19], [20], [21], [22], the data spatiality was generally referred to as the coverage of sensors. Most of them were concerned with the size of the coverage hole. However, this article concerned the distance between the query location and the closest sensor to the query location. As shown in Fig. 1, consider the following two cases with the same total size of the holes. In case 1, there is a big hole with size x. In case 2, there is a sensor s whose sensing range breaks the big hole into two smaller holes with the same size $x/2$. Let l_s denote the location of sensor s. Most related works considered that the two cases are identical since the total size of the coverage hole is identical. However, this article considers that case 2 has better spatial quality than case 1. The reason is stated in the following. Let $d_i(y, l_s)$ denote the distance between the query location and the sensor s, where i has value 1 or 2, denoting case 1 or 2, respectively. In the worst case, it is obvious that $d_1(y, l_s) > d_2(y, l_s)$. In this article, the spatial quality is impacted by the distance between the query location and the reporting sensor.

In addition to the spatial quality, this article also proposes the novel idea of temporal quality. As shown in Fig. 2, assume that sensor s is placed at location b. Consider the following two cases. In case 1, the sensor s performs sensing tasks at t_1^1 and t_2^1 time points with a sensing frequency λ_1. In case 2, the sensor s performs sensing tasks at t_1^2 and t_2^2 time points with

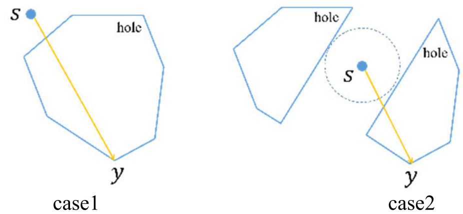

Fig. 1. Interpretation of spatial data quality.

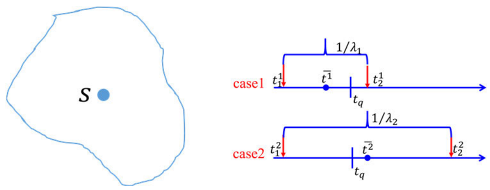

Fig. 2. Interpretation of temporal data quality.

a sensing frequency λ_2, where $\lambda_2 = (1/2)\lambda_1$. Assume that there is a query for the sensing data of the time point t_q. The WSN system will report the data collected at time points t_2^1 and t_1^2 in cases 1 and 2, respectively. This is because sensing time points t_2^1 and t_1^2 are closest to the query time point t_q. The temporal quality is defined by the time difference between the query time point and the closest sensing time point. Since $|t_1^2 - t_q| > |t_2^1 - t_q|$, the WSN in case 1 has better temporal quality than in case 2. In this article, each sensor will locally adjust its sensing frequency to achieve the maximal temporal quality, while its remaining energy can support the sensing task until the mobile charge comes to recharge the sensor. To our knowledge, this is the first study that considers both temporal and spatial qualities in developing the recharging mechanism.

B. Improving the Lowest Data Quality

Most existing recharging mechanisms [18], [19], [20], [21], [22] did not consider the lowest data quality. This article further analyzes the bottleneck location, which has the lowest data quality. When sensors are fully charged, the sensor with the lowest energy consumption rate will move to the bottleneck location. Compared with studies [18], [19], [20], [21], [22], the proposed algorithm further improves the lowest data quality of the monitoring region.

C. Improving the Recharging Efficiency

This article divides the monitoring area into several subregions and sets up a virtual recharging station in each subregion. All sensors in the same subregion should move to the virtual recharging station for recharging by the mobile charger. This can reduce the recharging path and cut down the recharging cost of the mobile charger. In addition, the mobile charger can recharge multiple sensors at the same, time which increases the recharging revenue, improving the recharging efficiency. The experimental studies also examine the improvements of this work, against the existing studies in terms of mobile charger efficiency index (MCEI).

The rest of this article is organized as follows. Section II reviews the existing studies. Section III introduces the network environment and related models, as well as formulates the problem investigated in this article. Section IV presents the experimental studies and results. Finally, the conclusion is drawn in Section VI.

II. Related Works

The following reviews the studies [15], [16], [17], [18], [19], [20], [21], [22], which developed the recharging technologies for WSNs. In addition, studies [12], [13], [14] proposed essential localization and coverage algorithms for the MWSNs. However, they did not take into consideration the recharge and data quality. Since this article develops a recharging mechanism in MWSNs, existing studies [12], [13], [14], which presented the characteristics and the cooperation between the mobile sensors, are also reviewed. The existing developed wireless charging technologies can be divided into two categories: offline and online.

A. Offline Schedule

In the offline category, the mobile charger did not change the recharging schedule even though it received new recharging requests from sensors. Xu et al. [15] proposed a wireless recharging algorithm that aimed to maximize the sum of all sensor lifetimes by partially charging the sensors while minimizing the charging path for the mobile charger. It proposed a recharging model for partial recharging of the requested sensors and then scheduled the mobile charger according to the energy consumption of each requested sensor. However, compared with the full recharging techniques, the partial recharging technique increased the path length cost of the mobile charger.

Shu et al. [16] proposed the speed control method of the mobile charger, aiming to maximize the lifetime of wireless rechargeable sensor networks (WRSNs). The waiting time for recharging between the two recharged sensor nodes determined the traveling speed of the mobile charger. It not only considered the linear recharging path but also considered the irregular charging path. Although this study maximized the recharged energy, it did not consider the data quality. Furthermore, the mobile charger adopted the offline policy, which did not consider the new requests. As a result, the recharging efficiency is lower than that of the studies that adopted the online strategy.

Fu et al. [17] proposed an offline recharging algorithm, called energy-synchronized mobile charging (ESync). Based on the different energy consumption of each sensor, it only recharged the sensors with low remaining energy. This study built the nested traveling salesman problem recharging rounds, aiming to reduce the recharging path of the mobile charger. In addition, the synchronization question was investigated, aiming to cut down the recharging delay of sensors. However, similar to study [16], study [17] also did not consider the data quality. In addition, it adopted the offline policy, resulting in inefficiency in terms of the path length.

B. Online Schedule

In general, the online schedule outperforms the offline schedule in terms of recharging efficiency. It is because the online schedule reduces the traveling path of the mobile charger by timely considering the sensors that sent the new requests. Han et al. [18] proposed a typical online recharging algorithm for WRSN. It partitioned the sensors into different clusters according to the predefined cluster radius. Then, it constructed the recharging schedule by considering the location and residual energy of the requested sensors. If the number of sensors that have already sent the recharging requests exceeded the threshold value, the base station would arrange multiple mobile chargers to execute the recharging tasks. Though this study extended the lifetime of WRSNs, it did not consider the data quality. In addition, each sensor is static in the considered WRSN. It is time-consuming for the mobile charger to visit each requested sensor.

Tian et al. [19] proposed a recharging algorithm that aimed to improve energy efficiency. The monitoring region was divided into a lot of hexagonal cells. Sensors in the hexagon formed the cluster. The mobile charger recharged the sensors in each cluster. According to the residual energy, sensors were sorted into three types. This study calculated the weight of the cluster based on the types of sensors. The mobile charger recharged the cluster in descending order of weight. In addition, the recharging path of the mobile charger was constructed by using the nearest neighbor algorithm. Although this study reduced the recharging path of the mobile charger, it did not consider the contribution of sensors and data quality.

Chen et al. [20] proposed the dual-side recharging scheme aiming to reduce the recharging path of the mobile charger and the total recharging energy. It assumed that each sensor had a different battery capacity. According to the residual energy, the battery capacity of each sensor, as well as the distance between sensors, it calculated the weight of each sensor. The power diagram was constructed based on the weights of the sensors. According to the power diagrams, the recharging path of the mobile charger was planned. The mobile charger could simultaneously recharge the sensors and collect the sensing data. However, it only considered the recharging efficiency. The data quality was not considered.

Tian et al. [21] proposed a recharging scheme to ensure efficient recharging and minimal charging cost. According to the distance between the sensors and the base station, it divided the sensors into two types: ring 0 and the out ring. The sensors in the set of ring 0 were recharged first by the mobile charger in a one-to-one manner. Then, the sensors in the outer ring were recharged later in a one-to-many manner to improve recharging efficiency. In addition, it applied the Hungarian algorithm to ensure that the sum normalized dead time is minimum, aiming to maximize the lifetime of the network. Finally, the mobile charger adjusted the recharging time slots of the sensors and then selected the sensor nodes closest to themselves to recharge. As a result, the total recharging path of the mobile charger can be shortened. However, the data quality was not considered in this study. It is time-consuming for the mobile charger to visit each requested sensor since each sensor is static in the considered WRSNs.

Yu et al. [22] investigated the issue of network coverage. It calculated the coverage benefit based on the coverage contribution of each sensor and the path cost of the mobile charger and then constructed the recharging path based on the coverage benefit. The purpose of this study was to improve the recharging efficiency and maximize the coverage of the network. However, it only investigated the issue of coverage, without considering the spatial data quality, temporal data quality, and the lowest data quality.

Although studies [18], [19], [20], [21], [22] developed online wireless recharging technologies, they did not consider both the spatial data quality and the temporal data quality. In comparison, this article considers the data quality and the recharging efficiency when developing the recharging mechanism.

Most studies [12], [13], [14] related to MWSN have investigated issues, including energy consumption, localization, sensor deployment, and target coverage. However, they did not take into consideration the recharge and data quality issues. These studies assumed that mobile sensors can move and the localization mechanisms can help mobile sensors be aware of their locations. This article aims to develop a recharging mechanism for the MWSN where all sensors are mobile. The monitoring region can be partitioned into several subregions and one recharging location will be determined for each subregion. In each subregion, all sensors will move to the recharging station and then be recharged by the mobile charger simultaneously. As a result, the mobile charger can move along a shorter traveling path and have better recharging efficiency. Table I summarizes the comparisons of the proposed mechanism with the related studies.

In general, the online schedule means that the mobile charger can adaptively change its recharging schedule according to the new requests sent from sensors, that is, the mobile charger and the sensors can be highly interactive when the mobile charger performs the recharging task. In this article, the mobile charger and the sensors are also highly interactive. The recharging schedule, including the locations of recharging stations and the arrival time point, made by the mobile charger, has been determined. Therefore, all sensors should adaptively adjust their sensing frequency to satisfy the following three conditions.

1) Reserve the remaining energy for the movement from its current location to the recharging station.
2) Arrive at the recharging station on time.
3) Utilize all its remaining energy for executing sensing operations, aiming to achieve the best temporal quality.

III. Network Environment and Problem Formulation

For a given MWSN, this article proposes a recharging scheduling algorithm that aims to maximize the data quality of the given monitoring region R. The following first introduces the network environment and energy consumption model for the mobile charger and sensors. Then, the spatial and temporal data qualities models are proposed. Finally, the problem formulation of this study is presented.

A. Network Environment

This article considers a rectangle monitoring region R with size $L \times W$, where L and W are the length and width of R, respectively. In the monitoring region, there is a sink station that plays the role of the data center and the static recharging station. Initially, the mobile charger is full of energy and stays

TABLE I
COMPARISONS OF THE PROPOSED MECHANISM WITH THE RELATED STUDIES

Related work	Issue	Recharging efficiency	Spatial data quality	Temporal data quality	Maximizing the lowest data quality	Sensor mobility
[12]	Energy consumption	×	×	×	×	○
[13]	Localization	×	×	×	×	○
[14]	Sensor deployment and target coverage	×	×	×	×	○
[15]	Recharge	low	×	×	×	×
[16]	Recharge	low	×	×	×	×
[17]	Recharge	low	×	×	×	×
[18]	Recharge	low	×	×	×	×
[19]	Recharge	low	×	×	×	×
[20]	Recharge	low	×	×	×	×
[21]	Recharge	low	×	×	×	×
[22]	Recharge	low	×	×	×	×
The proposed mechanism	Recharge	high	○	○	○	○

in the sink station. In the region R, it is assumed that a set of n sensors, denoted by $S = \{s_1, s_2, \ldots, s_n\}$, are randomly deployed over the monitoring region. Let DQ denote the term of data quality. The sensors are responsible for executing the sensing task, aiming to maximize the DQ.However, a big challenge for sensors is that they are battery-powered. To maintain a sustainable life, they should be recharged by the mobile charger before energy exhausting. Since the number of sensors is large, it is time-consuming for the mobile charger to visit each sensor and recharge it. A good recharging algorithm needs to determine the number and locations of the recharging stations. Then, the mobile charger only needs to visit each recharging station, instead of visiting each sensor. When the sensor needs to be recharged, it can move to the closest recharging station for recharging, saving the traveling time for the mobile charger to visit each sensor and recharge it.

Let T_{round} denote a round that is the period required for the mobile charger to leave from the sink station, visit each recharging station, and then finally return to the sink station. When the mobile charger visits each recharging station, it performs two tasks, including supplying the energy to the sensors that stay at the recharging station and collecting data from sensors. After returning to the sink station, the mobile charger will transmit the collected data to the sink station. The mobile charger will perform its recharging task round by round to supply the energy to all mobile sensors and collect data from sensors to the sink station.

Each mobile sensor performs the sensing task at a specific location. However, a certain level of battery energy needs to be reserved for moving from the current location to the closest recharging station to recharge its energy before the mobile charger will transmit the collected data to the sink station. The mobile charger will perform its recharging task round by round to supply the energy to all mobile sensors and collect data from sensors to the sink station.

Each mobile sensor performs the sensing task at a specific location. However, a certain level of battery energy needs to be reserved for moving from the current location to the closest recharging station to recharge its energy before the mobile sensor arrives at the recharging station. The mobile sensors can transmit their sensing data to the mobile charger during the recharging process. After fully recharged, the mobile sensors return to the sensing position for executing sensing work.

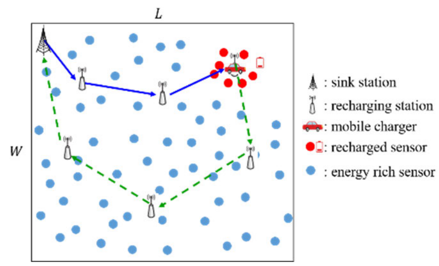

Fig. 3. Scenario of the considered network.

To guarantee that the collected data are fresh, the value of T_{round} should be bounded with a maximal value. This also implies that the number of recharging stations has an upper bound. Fig. 3 gives a scenario of the considered network. The sink station is located at the top-left corner. The blue nodes denote the energy-rich sensors, while the red nodes denote the sensors that are currently recharged by the mobile charger. The blue path presents the trajectory of the mobile charger, while the green dotted path presents the scheduled path in the near future. As shown in Fig. 3, when the mobile charger arrives at the third recharging station, all the sensors marked in red ink also arrived at the station ready for recharging their energies.

The DQ depends on several parameters of the mobile charger and sensors. The energy capacity, recharging rate, and speed of the mobile charger will impact the path length and the movement time of the mobile charger. On the other hand, the energy consumption for movement, sensing, and communication and the battery capacity of each mobile sensor also highly impact the DQ. To completely describe the parameters, the energy consumption model for the mobile charger and sensors is presented in Section III-B. The nomenclature lists the main notations in this article.

B. Energy Consumption Model for the Mobile Charger and Sensors

Assume that the mobile charger M has rich energy and the energy recharging issue for mobile charger M is ignored. It is easy to satisfy the assumption since another mobile charger that is fully recharged by the sink station can wait at the sink station and replace the returning mobile charger. Let e_M^{char} and $e_M^{\text{move\_disch}}$, respectively, denote the recharging rate and moving discharging rate of the mobile charger, which are two fixed values. In addition, mobile charger M moves at a constant speed, denoted by v_M.

Each sensor is mobile and can move to the recharging station for recharging its energy and then move back to the proper location for executing the monitoring task. Let E_{sensor} be the battery capacity of each sensor. Let v_s denote the moving speed of each mobile sensor. Let $e_s^{\text{move\_disch}}$ denote the energy discharging rate for each mobile sensor moving for one unit distance.

Different sensors have different working discharging rates since they are heterogeneous. Each sensor might be responsible for a different sensing task and therefore is embedded with different types of sensing elements. Let $e_k^{\text{work\_disch}}$ denote the energy discharging rate of the sensor s_k for working. Let f_k denote the sensing frequency of the sensor s_k.

The mobile charger transmits its power to the sensors in the way of wireless energy transmission. There are a lot of schemes of wireless energy transmission, such as electromagnetic induction coupling, electromagnetic radiation, and magnetic resonant coupling (MRC) [23]. The magnetic resonance coupled wireless transmission technology transmits energy from a sender coil to the receiver coil through strong coupling between two resonant coils at the same resonance frequency by nonradiative magnetic fields. Recent arts in MRC show that multiple sensors can be charged simultaneously. Angurala et al. [23] and [24] illustrated how the unmanned aerial vehicle (UAV) recharged the sensors using MRC. The proposed algorithm mainly adopts MRC technology to recharge the sensors.

The mobile charger can recharge the multiple sensors simultaneously, as long as they are within the recharging range of the mobile charger. Let D_M denote the recharging distance of the mobile charger. The notation D_M is mainly determined by the power reception rate of sensors, which should be larger than the threshold value ϱ. The power reception rate will be decreased with the distance between the sensor and the mobile charger. In the experiments, we refer to the experiment data in [25], and the recharging distance of the mobile charger is set at 5 m. If the sensor is outside the recharging range of the mobile charger, the power reception rate is too low to recharge the sensor.

Let E_k^{ford} denote the energy consumption for the sensor s_k moving from its current location to the recharging location. Let E_k^{back} denote the energy consumption for the sensor s_k moving from the recharging location to its working location. The energy of a sensor is used for moving to the recharging location and working, which includes sensing, receiving, and transmitting data. Suppose that the size of a packet is h bits. Let d_{kg} denote the Euclidean distance of the sensor s_k and sensor s_g. Let E_k^r denote the energy consumption of receiving one packet of data. The value of E_k^r can be obtained by

$$E_k^r = h \times \alpha \tag{1}$$

where parameter α denotes the energy consumption of the receiving circuit for 1 bit.

Let E_k^t denote the energy consumption for the sensor s_k to transmit one packet to the mobile charger or sensor s_g. Let η_1 and η_2 denote the energy consumption of the transmitting circuit and the amplifier circuit for 1 bit, respectively. The following equation calculates the value of E_k^t:

$$E_k^t = h \times \eta_1 + h \times d_{kg}^2 \times \eta_2. \tag{2}$$

Let E_k^s denote the energy consumption of sensing one packet of data. Let $E(s_k)$ denote the total energy consumption of the s_k in the round. The value of $E(s_k)$ can be obtained by applying the following equation:

$$E(s_k) = E_k^r + E_k^t + E_k^s + E_k^{\text{ford}} + E_k^{\text{back}}. \tag{3}$$

After describing the energy consumption parameters of the mobile charger and sensors, Section III-C will discuss the DQ model, which consists of spatial and temporal DQ.

C. Spatial and Temporal Data Qualities Models

The DQ of a given monitoring area can be measured from two points of view: spatial and temporal qualities. Consider a humidity sensor that is deployed at a certain location a. Assume that the sensor s performs sensing operation and detects the humidity value 76% at time t. It is appreciated to use humidity = 76% to estimate the humidity of locations x_{loc} which are close to a. Therefore, the DQ of the location x_{loc} is high if the data collected at the location a are used to represent the data of the location x_{loc} even though location x_{loc} did not deploy the sensor. However, it is not appreciated to use humidity = 76% to represent the humidity of locations y_{loc}, which is far away location a. Therefore, the DQ of the location y_{loc} is low. The explanation of the abovementioned two cases implies that the DQ has a *spatial locality*.

Similarly, the following illustrates that the DQ also has a *temporal locality*. Let us consider location a. It is appreciated to use humidity = 76% to estimate the humidity at the time x_{time}, which is close to time point t, where $x_{\text{time}} > t$. Therefore, even though the sensor s did not perform sensing operation at the time x_{time}, it is appreciated to use sensing data humidity = 76%, which is collected at time point t to represent the humidity at time point x_{time}. However, it is not appreciated to use humidity = 76% to represent the humidity at the time y_{time}, which is far away from time point t. Therefore, the DQ also has a temporal locality.

Fig. 4(a) shows the deployment of RSs in the monitoring region. Let notation s.loc denote the location of the sensor s. In Fig. 4(a), the region R has been partitioned into several Voronoi cells according to the location s.loc of each sensor $s \in S$. Let R_s denote the Voronoi cell of sensor s. As shown in Fig. 4(b), the polygon, which surrounds sensor s, is the Voronoi cell R_s of sensor s, that is, all space points in R_s have the following property:

$$s = \min_{s_i \in S} \text{dist}(s_i, p), \quad \text{for } \forall p \in R_s.$$

Therefore, the data collected by the sensor s will be used to represent the data of any point $p \in R_s$. Fig. 4(c) further shows

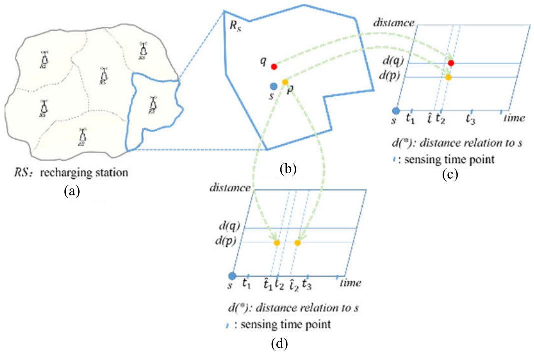

Fig. 4. Example of the spatial and temporal qualities. (a) Deployment of *RSs* in the monitoring region. (b) Voronoi cell R_s of sensor s. (c) Space relation of point p, q, and sensor s. (d) Time relation of point p and sensor s.

the space–time relation of each point $p \in R_s$ and the sensor s. As shown in Fig. 4(c), the sensor s executes sensing operations at time points t_i. For example, the sensor s executes sensing operations at t_1–t_3 but does not execute the sensing operation at $\hat{t}$. For each space point $p \in R_s$, it has a distance relation $d(p)$, which returns the distance of sensor s and p. Each space point p can be mapped from Fig. 4(b) to (c) and Fig. 4(b) to (d), which represent the view of space–time relations of point p and the sensor s. This view is very important for measuring the DQ of point p since data collected by the sensor s will be used to present the data of point p.

The following presents the space and time localities of surveillance by using two points p and q as an example. Consider two points p and q in the Voronoi cell R_s of sensor s. Since there is no sensor deployed at locations p and q, it is straightforward to use data collected at location s.loc to represent the data of locations p and q. The following aims to present the spatial locality impact on the DQ of points p and q. Consider the DQ of points p and q at a certain time t_2, which is the time point that the sensor s executes the sensing operation. As shown in Fig. 4(c), the following distance relation holds:

$$d(p) < d(q).$$

According to the spatial locality, the DQ of p is higher than that of q because p is relatively close to sensor s compared to q. Fig. 4(d) further shows the impact of temporal locality on DQ. Consider space point p and two-time points $\hat{t}_1$ and $\hat{t}_2$ in Fig. 4(d). Since sensor s does not execute the sensing operation at time points $\hat{t}_1$ and $\hat{t}_2$ and the time point t_2 is the closest sensing time point to both the time points $\hat{t}_1$ and $\hat{t}_2$, it is straightforward to use sensor data collected by sensor s at the time t_2 to represent the sensing data of point p at time points $\hat{t}_1$ and $\hat{t}_2$. Comparing $\hat{t}_1$ and $\hat{t}_2$, $\hat{t}_2$ is closer to the time point t_2. Therefore, we have

$$|\hat{t}_1 - t_2| < |\hat{t}_2 - t_2|.$$

According to the temporal locality, the DQ of point p at the time point $\hat{t}_1$ is higher than that of the time point $\hat{t}_2$. The impacts of spatial and temporal localities on DQ are similar to the impact of pheromone on the ant. Therefore, this article adopts the ant pheromone impact to calculate the spatial and temporal qualities of all the sensors in the given network.

The following formally defines the DQ of any point $p \in R$. Recall that R_{s_k} denotes the Voronoi cell of the sensor s_k. Assume that space point $p \in R_{s_k}$, that is, the sensor s_k satisfies the relation

$$s_k = \arg\min_{s \in S} \operatorname{dist}(s, p).$$

Therefore, the data collected by the sensor s_k will be used to represent the data of any point $p \in R_{s_k}$.

Let $d(s_k, p)$ denote the Euclidean distance of the sensor s_k and p. Assume that the coordinates of s_k and p are $(x_{k,} y_k)$ and $(x_{p,} y_p)$, respectively. The distance $d(s_k, p)$ can be calculated by

$$d(s_k, p) = \sqrt{(x_k - x_p)^2 + (y_k - y_p)^2}.$$

Let r_s denote the sensing radius of the sensor s_k. Let $\delta_{k,p}^t$ denote whether or not p is within the coverage of s_k at any time point t

$$\delta_{k,p}^t = \begin{cases} 1, & d(s_k, p) \le r_s \\ 0, & \text{otherwise.} \end{cases} \tag{4}$$

The following defines the Boolean variable λ_k^t, which represents the two states of the sensor node at time point t

$$\lambda_k^t = \begin{cases} 1, & \text{sensor } s_k \text{ is monitoring at time} t \\ 0, & \text{otherwise.} \end{cases} \tag{5}$$

For convenience, the following uses temporal-DQ and spatial-DQ to denote the temporal and spatial data qualities, respectively. Let $\varphi_{p,t}^{\text{temporal}}$ and $\varphi_{p,t}^{\text{spatial}}$ denote the temporal-DQ and spatial-DQ of p at time t, respectively, in the monitoring region R. Let $\varphi_{p,t}$ denote the DQ, including $\varphi_{p,t}^{\text{temporal}}$ and $\varphi_{p,t}^{\text{spatial}}$. When measuring DQ of point p, four possible cases should be discussed as follows.

Case I: $\delta_{k,p}^t = 1$ and $\lambda_k^t = 1$.

In this case, space point p falls in the coverage of s_k, and s_k executes sensing operation at time t. Since this is the best case, the DQ $\varphi_{p,t}$ of point p at time point t is $\varphi_{p,t} = 1$.

Case II: $\delta_{k,p}^t = 1$ and $\lambda_k^t = 0$.

In this case, space point p falls in the coverage of s_k, and s_k does not execute the sensing operation at time t. However, the sensor executes the sensing operation at the time t_1, which is the closest sensing time point to time t. Let $d(t, t_1)$ denote the time difference between the last sensing time t_1 of s_k and the current time t. The difference $d(t, t_1)$ can be calculated by

$$d(t, t_1) = t_1 - t.$$

According to the ant pheromone, the loss of DQ of point p depends on the difference between the last sensing time of s_k and the current time t. The DQ $\varphi_{p,t}$ of point p at time point t is

$$\varphi_{p,t} = (1 - \sigma)^{d(t,t_1)} \tag{6}$$

where parameter σ denotes the loss rate of DQ per unit of time.

Case III: $\delta_{k,p}^t = 0$ and $\lambda_k^t = 1$.

In this case, the space point p does not fall in the coverage range of s_k, and s_k executes sensing operation at time t. Since sensor s_k is the closest sensor to point p, its sensing data will be used to represent the information of point p. According to the spatial locality discussed before, the loss of DQ of point p depends on the distance between the sensor s_k and point p. By applying the ant pheromone effect, the DQ $\varphi_{p,t}$ of point p at time point t is measured by

$$\varphi_{p,t} = (1-\varepsilon)^{d(p,s_k)} \tag{7}$$

where parameter ε denotes the loss rate of DQ per unit distance.

Case IV: $\delta_{k,p}^t = 0$ and $\lambda_k^t = 0$.

In this case, space point p does not fall in the coverage of s_k, and s_k does not execute the sensing operation at time t. However, sensor s_k is the closest sensor to point p and it executes the sensing operation at the time t_1, which is the closest sensing time point to time t. According to the spatial locality, the loss of DQ of point p depends on the distance between the sensor s_k and the point p. In addition, according to the temporal locality, the loss of DQ of point p depends on the difference between the last sensing time t_1 and the current time t. As a result, the data qualities $\varphi_{p,t}$ of point p at time point t are measured by

$$\varphi_{p,t} = (1-\varepsilon)^{d(p,s_k)} \times (1-\sigma)^{d(t,t_1)}. \tag{8}$$

Let Q denote the DQ of the whole monitoring region in period T. The value of Q is presented by the following equation, which is the average of the DQ of all possible points in $p \in R$ and all-time points $t \in T$:

$$Q = \frac{\sum_{p\in R}\sum_{t\in T}\varphi_{p,t}}{|R||T|}. \tag{9}$$

D. Problem Formulation

This article addresses the issue of DQ for a given MWSN.

The objective of this article is to propose a recharging scheduling algorithm for the mobile charger and mobile sensors, aiming to maximize the DQ of the monitoring region R. To deal with this issue, the developed algorithm should determine the number of recharging stations, the locations of these stations, as well as the location assignments of all recharged sensors. Herein, it is noticed that the mobile charger and sensors only need to know the location of each recharging station. It is no need to set up any deployment or any physical object at each recharging station. This article aims to propose an algorithm A_j for maximizing the DQ of R. A_j is presented by

$$A_j = (b, L_{\text{charger}}, P, L_{\text{sensor}})$$

where b denotes the number of recharging stations, L_{charger} denotes the set of locations of recharging stations, P denotes the recharging path of the mobile charger, and L_{sensor} denotes the location mapping, which maps each recharged sensor to the working location.

The following presents the objective function and the constraints of the mobile sensor network.

Objective Function:

$$Q = \max_{A_j\in A}\frac{\sum_{p\in R}\sum_{t\in T}\varphi_{p,t}}{|R||T|} \tag{10}$$

where A denotes the set of all possible algorithms. This article aims to develop an algorithm to maximize the data quality of the monitoring area. The data quality considers two aspects: spatial and temporal data qualities. To improve the spatial data quality, the mobile charger should recharge those sensors that have higher contributions in terms of spatial quality. In addition, the sensors should make the best energy management such that they can perform the sensing operations at right time for achieving the best temporal quality. Therefore, the goal of this article is to develop an algorithm for achieving the best spatial and temporal qualities. Expression (10) reflects the goal of this article.

Some constraints given below should be satisfied. The first constraint is the data freshness constraint. The mobile charger stops at each recharging location, recharges some sensors, collects their sensing data simultaneously, moves along the path, and finally returns to the sink station. Then, the mobile charger will transmit all collected data to the sink station. Let T_M^{move} denote the total time required for the mobile charger to move along the recharging path. Let T_M^{ch} denote the total time required for recharging the sensors at all recharging stations. Let T_M denote the predefined time, which is a threshold value of data freshness. Expression (11) gives the data freshness constraint, which ensures that the data received by the sink station are fresh enough, that is, the total time T_{round}, including the movement time T_M^{move} and recharging time T_M^{ch} of each round, should be small than or equal to the threshold value T_M. The following constraint reflects the data freshness constraint.

E. Data Freshness Constraint

$$T_{\text{round}} = T_M^{\text{move}} + T_M^{\text{ch}} \le T_M. \tag{11}$$

Another constraint is that the energy of the mobile charger should be enough for executing the recharging task in each round T_{round}. Recall that the main tasks of the mobile charger are to visit each recharging station, execute the recharging task, and receive data from sensors. Finally, the mobile charger will return to the sink station and transmit its data to the sink station. Let E_{charger} denote the battery capacity of the mobile charger. Let δ denote the energy required to communicate with sensors and the sink station. Let E_M^{move} and E_M^{ch} denote energies required for the mobile charger moving along the recharging path and recharging sensors at all recharging stations, respectively. Compared with E_M^{move} and E_M^{ch}, the value of δ is very small. Expression (12) gives the mobile charger energy constraint.

F. Mobile Charger Energy Constraint

$$E_{\text{charger}} \ge E_M^{\text{move}} + E_M^{\text{ch}} + \delta. \tag{12}$$

Another constraint is that the battery of each sensor s_k should satisfy the total energy consumption of that sensor. The following sensor energy constraint reflects this requirement.

G. Sensor Energy Constraint

$$E(s_k) = E_k^r + E_k^t + E_{s_k}^s + E_k^{\text{ford}} + E_k^{\text{back}} < E_{\text{sensor}}. \quad (13)$$

Another constraint, called *the recharging efficiency constraint*, should be satisfied. As shown in (14), this constraint guarantees that the sensor energy is majorly consumed for working, rather than for movement. Herein, it is noticed that each sensor is mobile and should move to the recharging station for energy supplements. This constraint guarantees that the remaining energy of each sensor should be much greater than the energy consumption for movement. Let E_k^{rem} denote the total energy of the sensor s_k for working. The following constraint reflects the recharging efficiency constraint.

H. Recharging Efficiency Constraint

$$E_k^{\text{rem}} \gg E_k^{\text{ford}} + E_k^{\text{back}}. \quad (14)$$

Section IV presents the proposed recharging scheduling algorithm, which aims to achieve our objective function given in (10) while satisfying the constraints (11)–(14).

IV. Algorithm Description

This article presents the algorithm aiming to maximize the DQ of region R. The algorithm consists of three phases: initial phase (IN Phase), working phase (WR Phase), and recharging phase (RC Phase). In the IN Phase, the mobile charger needs to partition the monitoring region into several equal-sized subregions to simplify the issue of determining the number and locations of recharging stations. Then, mobile charger will calculate the starting recharge time of each subregion and broadcast the starting recharge time points to all sensors in the monitoring region R. In the WR Phase, each sensor executes its sensing task and calculates working time based on the starting recharge time of the subregion where the sensor is located. In addition, each sensor will calculate the sensing frequency, aiming to achieve the maximal *temporal-DQ*. In the RC Phase, the mobile charger recharges all sensors that have already stayed at some recharging stations and then dispatches these sensors to the working locations according to their energy consumption rates.

A. Phase I: IN Phase

This article assumes that the monitoring area is divided into m^2 (m is an even number) equal-sized subregions. The center location of each subregion will be virtually considered as the recharging station. Herein, we notice that this location is only the estimated recharging location for predicting the number of recharging stations. The real locations will be determined in the later phase. Let R_i^{sub} denote the ith subregion. Let RS_i denote the center point of the subregion R_i^{sub}, which is also the location of the recharge station in that subregion. In particular, RS_1 denotes the sink station, which is the fixed recharge station in R_1^{sub} for the mobile charger to supply its energy.

The proposed algorithm aims to maximize the data quality of the monitoring region. The sensors arrive at the recharging station at the appointed time and are recharged by the mobile charger. However, the number and the location of recharging stations are uncertain. The major constraint is that the energy of the mobile charger should completely support both the moving along the constructed path and recharging sensors at each recharging station. In case the path is dynamically changed, it is difficult to predict the energy required for moving. It will lead to difficulty to measure the number of recharging stations. To simplify the abovementioned problems, this article applies the snake-like path such that it is easy to calculate the energy required for moving if the size of each subregion is determined. To evaluate the number of recharging stations, the simplest way is to use the snake-like path to measure the required energy for moving. Then, the remaining energy can be used to measure the number of recharging stations since the energy consumed for recharging sensors in each station can be calculated. The final path of the mobile charger is also snake-like. The path will be constructed in a snake-like manner, as shown in Fig. 5.

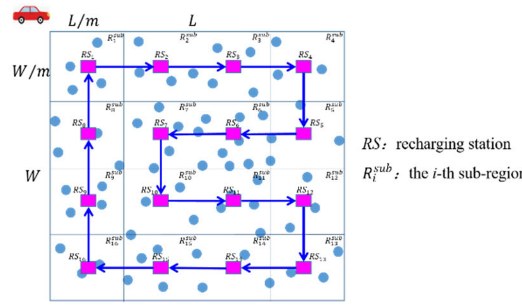

Fig. 5. Recharging path of the mobile charger.

Let $S_i = \{s_1^i, s_2^i, \ldots, s_{|S_i|}^i\}$ denote the set of sensors located in subregion R_i^{sub}. Let L/m and W/m denote the length and width of each subregion, respectively. The movement time T_M^{move} of the mobile charger can be obtained by the following:

$$\begin{aligned} T_M^{\text{move}} &= \frac{\sum_{i=1}^{m^2} d\left(\text{RS}_i, \text{RS}_{(i+1)\text{mod}(m^2)}\right)}{v_M} \\ &= \frac{2(m-1) \times L/m + 2(m-1) \times W/m + (m-2)^2 \times L/m}{v_M}. \end{aligned} \quad (15)$$

To reserve as much as possible energy for sensors working in R_1^{sub}, this article assumes that the starting time for recharging at the first subregion will be the time point that the last sensor arrives at the RS. Another assumption is that the energy of each sensor is exhausted when each sensor arrives at the RS. Hence, the required recharging time of the subregion R_i^{sub} is equal to the battery capacity of the sensor divided by the recharging rate of the mobile charger. Let T_i^{ch} denote the required recharging time of the subregion R_i^{sub}. The value of T_i^{ch} can be obtained by the following:

$$T_i^{\text{ch}} = \frac{E_{\text{sensor}}}{e_M^{\text{char}}}. \quad (16)$$

The total time T_M^{ch} required for recharging all sensors at all RSs can be calculated by the following accordingly:

$$T_M^{\mathrm{ch}} = \sum_{i=1}^{m^2} T_i^{\mathrm{ch}}. \tag{17}$$

To satisfy the data freshness constraint, the sum of T_M^{move} and T_M^{ch} should be small than or equal to the threshold value of data freshness T_M, i.e.,

$$\frac{2(m-1)\times L/m + 2(m-1)\times W/m + (m-2)^2 \times L/m}{v_M} + \sum_{i=1}^{m^2} T_i^{\mathrm{ch}} \le T_M. \tag{18}$$

Let $m^{\max}$ be the largest value that satisfies (18). The next task of the IN Phase is that the mobile charger should calculate the starting recharge time points of all subregions and broadcast them to all sensors in R. To achieve this, the mobile charger collects the ID, location, and discharging rate of each sensor in the first subregion. This information helps the mobile charger to calculate the starting recharge time point of the first subregion. Then, the starting recharge time of the next subregion, say RS_{i+1}, could be easily obtained by adding the recharging time of the sensors in RS_i plus the movement time required from RS_i to RS_{i+1}.

The following presents the calculation of the starting recharge time of RS_1. The mobile charger will broadcast the calculated starting recharge time to all sensors in the first subregion. Recall that $S_1 = \{s_1^1, s_2^1, \ldots, s_{|S_1|}^1\}$ denotes the set of sensors in the first subregion R_1^{sub}. Let $\mathrm{L}_i^{\mathrm{old}} = \{l_1^{\mathrm{old},i}, l_2^{\mathrm{old},i}, \ldots, l_{|\mathrm{L}_i^{\mathrm{old}}|}^{\mathrm{old},i}\}$ denote the set of original locations of $s_k^i \in S_i$, where $l_k^{\mathrm{old},i}$ denotes the original location of the sensor s_k^i in subregion R_i^{sub}. Let $T_k^{\mathrm{move,initial}}$ denote the time required for the sensor s_k^1 moving from its working location to the recharging station RS_1. Let $d(l_k^{\mathrm{old},1}, \mathrm{RS}_1)$ denote the Euclidean distance of s_k^1 and the recharging station RS_1. Let $E_k^{\mathrm{move,initial}}$ denote energy consumption required for the sensor s_k^1 moving from the working location to the recharging station RS_1. The following equations calculate the time $T_k^{\mathrm{move,initial}}$ and energy consumption $E_k^{\mathrm{move,initial}}$, respectively

$$T_k^{\mathrm{move,initial}} = \frac{d(l_k^{\mathrm{old},1}, \mathrm{RS}_1)}{vs} \tag{19}$$

$$E_k^{\mathrm{move,initial}} = T_k^{\mathrm{move,initial}} \times e_s^{\mathrm{move\_disch}}. \tag{20}$$

The working energy, denoted by $E_k^{\mathrm{work,initial}}$, of sensor s_k^1 can be calculated by the following:

$$E_k^{\mathrm{work,initial}} = E_{\mathrm{sensor}} - E_k^{\mathrm{move,initial}}. \tag{21}$$

Let $T_k^{\mathrm{work,initial}}$ denote the working time of the sensor s_k^1. The energy discharging rate of the sensor s_k^1 for working is known, which is denoted by $e_k^{\mathrm{work\_disch,initial}}$. The value of $T_k^{\mathrm{work,initial}}$ can be obtained by applying the following equation:

$$T_k^{\mathrm{work,initial}} = \frac{E_k^{\mathrm{work,initial}}}{e_k^{\mathrm{work\_disch,initial}}}. \tag{22}$$

Let $T_k^{\mathrm{arrive,initial}}$ denote the time point that the sensor s_k^1 arrives at the recharging station RS_1. $T_k^{\mathrm{arrive,initial}}$ is calculated by the following:

$$T_k^{\mathrm{arrive,initial}} = T_k^{\mathrm{work,initial}} + T_k^{\mathrm{move,initial}}. \tag{23}$$

Let $T_i^{\mathrm{start\_recharge}}$ denote the starting recharge time of subregion R_i^{sub}. To fully utilize the remaining energy for the sensing task, the starting time for recharging at the first subregion will be the time point that the last sensor arrives RS_1. The following equation calculates the value of $T_1^{\mathrm{start\_recharge}}$:

$$T_1^{\mathrm{start\_recharge}} = \max_{s_k^1 \in S_1} \left(T_k^{\mathrm{arrive,initial}}\right). \tag{24}$$

Upon obtaining the starting recharge time of the first subregion, the starting recharge times of the other subregions can be calculated accordingly. The value of $T_i^{\mathrm{start\_recharge}}$ can be calculated based on the starting recharge time and recharged time of R_{i-1}^{sub} plus the moving time required from the subregion R_{i-1}^{sub} to the subregion R_i^{sub}, i.e.,

$$T_i^{\mathrm{start\_recharge}} = T_{i-1}^{\mathrm{start\_recharge}} + T_{i-1}^{\mathrm{ch}} + T_M^{\mathrm{move},i-1,i}. \tag{25}$$

Afterward, the mobile charger broadcasts the starting recharge time points $T_i^{\mathrm{start\_recharge}}$ of subregion R_i^{sub} to all sensors $s_k^i \in S_i$ for $1 \le i \le m^2$.

B. Phase II: WR Phase

In the IN-Phase, each sensor in the subregion R_i^{sub} has received the starting recharge time $T_i^{\mathrm{start\_recharge}}$. In the WR Phase, each sensor $s_k^i \in S_i$ will further calculate its working time based on $T_i^{\mathrm{start\_recharge}}$ such that sensors can arrive at RS_i on time and reserve maximal remaining energy for executing the sensing task. Another important goal in this phase is that each sensor $s_k^i \in S_i$ will calculate its sensing frequency, aiming to achieve the maximal *temporal-DQ*.

To calculate the working time, each sensor s_k^i should first reserve energy required for moving from the old working location $l_k^{\mathrm{old},i}$ to the recharging station RS_i. The following presents the calculation of the working time, which is derived from the calculations of the time required for moving between the working location and RS_i.

Let $E_k^{\mathrm{ford},i}$ and $T_k^{\mathrm{ford},i}$ denote the energy and the time required for the sensor $s_k^i \in S_i$ moving from its working location to the recharging station RS_i, respectively. The following equations calculate the values of $T_k^{\mathrm{ford},i}$ and $E_k^{\mathrm{ford},i}$, respectively

$$T_k^{\mathrm{ford},i} = \frac{d\left(l_k^{\mathrm{old},i}, \mathrm{RS}_i\right)}{vs} \tag{26}$$

$$E_k^{\mathrm{ford},i} = T_k^{\mathrm{ford},i} \times e_s^{\mathrm{move\_disch}}. \tag{27}$$

Let working energy $E_k^{\mathrm{rem},i}$ denote the total energy reserved for the sensor s_k^i to execute the sensing task at the location $l_k^{\mathrm{old},i}$. The value of $E_k^{\mathrm{rem},i}$ can be calculated by the following:

$$E_k^{\mathrm{rem},i} = E_{\mathrm{sensor}} - E_k^{\mathrm{ford},i}. \tag{28}$$

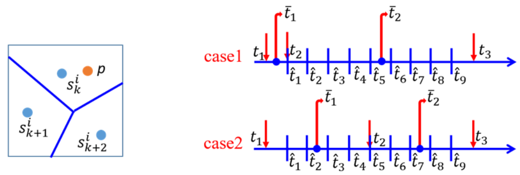

(a) (b)

Fig. 6. (a) Voronoi cells of the sensors s_k^i, s_{k+1}^i and s_{k+2}^i. (b) Regular-SF, and irregular-SF of the sensor s_k^i.

Let $T_k^{\text{departure},i}$ denote the departure time for recharging the sensor s_k^i. The following equation calculates the value of $T_k^{\text{departure},i}$:

$$T_k^{\text{departure},i} = T_i^{\text{start\_recharge}} - T_k^{\text{ford},i}. \tag{29}$$

Let $T_k^{\text{work},i}$ denote the working time of the sensor s_k^i. The value of $T_k^{\text{work},i}$ can be obtained by applying the following equation:

$$T_k^{\text{work},i} = T_k^{\text{departure},i}. \tag{30}$$

After obtaining the working time, the next task in this phase is to calculate the sensing frequency of each s_k^i, aiming to equally distribute the sensing time points over the period of working time and maximize the *temporal-DQ*. The following gives an example to illustrate the impact of sensing frequency on the *temporal-DQ*.

Fig. 6(a) shows a subregion and three sensors s_k^i, s_{k+1}^i, and s_{k+2}^i have been deployed in this subregion. The blue lines partition the subregion into three Voronoi cells. Let p be a point in the Voronoi cell of s_k^i. This indicates that the sensor s_k^i is the closest sensor of point p compared with the other two sensors. According to the concept of spatial locality, it is appreciated to use the sensing data of s_k^i to represent the sensing data of location p since there is no sensor deployed at location p.

Given a period T, let $\wp^T = (t_1, \ldots, t_\omega)$ denote a sensing frequency pattern with length ω, where t_i denotes the time point for executing the ith sensing operation in T, $1 \le i \le \omega$. Let $T_{i,i+1} = [t_i, t_{i+1}]$ denote the duration between time points t_i and t_{i+1}. The pattern $\wp^T$ is said to be a *regular sensing frequency* if $T_{i-1,i} = T_{i,i+1}$, for every $2 \le i \le \omega - 1$. On the contrary, the pattern $\wp^T$ is said to be *irregular sensing frequency* if it is not regular. For convenience, notations *Regular-SF* and *Irregular-SF* are used to shortly denote the terms regular and irregular sensing frequencies, respectively.

Fig. 6(b) shows two cases of *Regular-SF* and *Irregular-SF* for sensor s_k^i to execute the sensing task. Consider that the sensor s_k^i performs sensing operation in working period T.

1) Regular Frequency Feature: The sensor applying *Regular-SF* can obtain better *temporal-DQ* than it applying the *Irregular-SF*.

The following uses an example to illustrate the regular frequency feature. Assume that the sensor s_k^i executes the sensing operations at time points t_1–t_3. Consider the following two cases that adopt *Irregular-SF* in case 1 and *Regular-SF* in case 2.

In case 1, it is obvious that condition $T_{1,2} \ne T_{2,3}$ holds. Let $\bar{t}_1$ and $\bar{t}_2$ denote the midpoints of $[t_1, t_2]$ and $[t_2, t_3]$, respectively. Assume that $T_{1,3}$ is equally divided into ten segments. Let τ denote the length of each segment. Herein, we notice that time points $\hat{t}_i$, $1 \le i \le 5$, are closer to t_2, while time points $\hat{t}_i$, $6 \le i \le 9$, are closer to t_3. Let $\varphi_{p,t}^{\text{temporal},1}$ and $\varphi_{p,t}^{\text{temporal},2}$ denote the *temporal-DQ* of cases 1 and 2, respectively. The *temporal-DQs* of point p at time $\hat{t}_i$, $1 \le i \le 9$, can be calculated by applying (6), as shown in Table II.

In case 2, the sensor s_k^i adopts Regular-SF, that is, $T_{1,2} = T_{2,3}$. In the same way, the temporal surveillance qualities of point p at time points $\hat{t}_i$, $1 \le i \le 9$, are shown in Table III.

The sensor s_k^i executes sensing operations at time points t_1 and t_3. Therefore, the *temporal-DQ*s of point p at time points t_1 and t_3 are equal to 1. According to (9), $\varphi_{p,t}^{\text{temporal},1}$ is equal to the average of the *temporal-DQ* of all time points $t \in T_{1,3}$. In case 1, the *temporal-DQ* of point p at the period $T_{1,3}$ is calculated by the following:

$$\varphi_{p,t}^{\text{temporal},1} = \frac{3+2(1-\sigma)^{\tau}+2(1-\sigma)^{2\tau}+2(1-\sigma)^{3\tau}+2(1-\sigma)^{4\tau}}{|T_{1,3}|}. \tag{31}$$

In case 2, the *temporal-DQ* of point p at the period $T_{1,3}$ is calculated by the following:

$$\varphi_{p,t}^{\text{temporal},2} = \frac{3+4(1-\sigma)^{\tau}+4(1-\sigma)^{2\tau}}{|T_{1,3}|}. \tag{32}$$

Because of $0 \le \sigma \le 1$, the function

$$(1-\sigma)^{x\tau}, \quad 0 \le x \le 1$$

is a decreasing function. Therefore, $\varphi_{p,t}^{\text{temporal},2}$ is larger than $\varphi_{p,t}^{\text{temporal},1}$.

Based on the regular frequency feature, each sensor should equally distribute its sensing operations over the working period. Let $e_k^{\text{sensing},i}$ denote the energy consumption rate of the node s_k^i for each sensing operation. Let f_k^i denote the sensing frequency of the sensor s_k^i. Since the value of f_k^i is known, the value of $e_k^{\text{sensing},i}$ can be calculated by the following:

$$e_k^{\text{sensing},i} = e_k^{\text{work\_disch},i} \Big/ f_k^i. \tag{33}$$

Let ψ_k^i denote the total number of the sensing operations of s_k^i. The following equation calculates the value of ψ_k^i

$$\psi_k^i = \frac{E_k^{\text{rem},i}}{e_k^{\text{sensing},i}}. \tag{34}$$

Let $f_k^{\text{best},i}$ denote the best sensing frequency of s_k^i. Based on the regular frequency feature, the value of $f_k^{\text{best},i}$ can be obtained by applying the following equation:

$$f_k^{\text{best},i} = \psi_k^i \Big/ T_k^{\text{work},i}. \tag{35}$$

C. Phase III: RC Phase

In this phase, the mobile charger performs the recharging operation to support the energies of all sensors in each subregion. One of the major goals of this article is to maximize the *spatial-DQ* of the monitoring region R. Since sensors are randomly deployed in the monitoring area, they should be relocated to balance the sizes of Voronoi cells in each subregion.

TABLE II
TEMPORAL-DQ OF POINT P IN CASE 1

	$\hat{t}_1$	$\hat{t}_2$	$\hat{t}_3$	$\hat{t}_4$	$\hat{t}_5$	$\hat{t}_6$	$\hat{t}_7$	$\hat{t}_8$	$\hat{t}_9$
$\varphi_{p,t}^{temporal,1}$	$(1-\sigma)^0 = 1$	$(1-\sigma)^{\tau}$	$(1-\sigma)^{2\tau}$	$(1-\sigma)^{3\tau}$	$(1-\sigma)^{4\tau}$	$(1-\sigma)^{4\tau}$	$(1-\sigma)^{3\tau}$	$(1-\sigma)^{2\tau}$	$(1-\sigma)^{\tau}$

TABLE III
TEMPORAL-DQ OF POINT P IN CASE 2

	$\hat{t}_1$	$\hat{t}_2$	$\hat{t}_3$	$\hat{t}_4$	$\hat{t}_5$	$\hat{t}_6$	$\hat{t}_7$	$\hat{t}_8$	$\hat{t}_9$
$\varphi_{p,t}^{temporal,2}$	$(1-\sigma)^{\tau}$	$(1-\sigma)^{2\tau}$	$(1-\sigma)^{2\tau}$	$(1-\sigma)^{\tau}$	$(1-\sigma)^0 = 1$	$(1-\sigma)^{\tau}$	$(1-\sigma)^{2\tau}$	$(1-\sigma)^{2\tau}$	$(1-\sigma)^{\tau}$

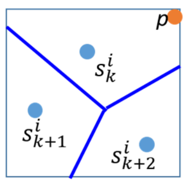

Fig. 7. Voronoi cell2 of the sensor s_k^i.

In the RC Phase, the relocation algorithm is presented for each subregion R_i^{sub}.

Let $\mathrm{L}_i^{\text{new}} = \{l_1^{\text{new},i}, l_2^{\text{new},i}, \ldots, l_{|\mathrm{L}_i^{\text{new}}|}^{\text{new},i}\}$ denote the set of relocated locations, where $l_k^{\text{new},i}$ denotes the relocated location of the sensor $s_k^i \in S_i$ in subregion R_i^{sub}. This article considers the energy consumption rate of each sensor as the key parameter to determine the relocated location of each sensor, aiming to maximize the *spatial-DQ*.

The following describes how the sensor s_k^i determines its working location after it finishes the recharging task. As shown in Fig. 7, point p is closer to the sensor s_k^i compared to s_{k+1}^i and s_{k+2}^i. Therefore, the sensing data of s_k^i will be used to represent the information of p. However, the *spatial-DQ* of p is determined by the distance between sensor p and s_k^i. If p is far away s_k^i, the *spatial-DQ* of p will be low.

To improve the *spatial-DQ* of all sensors in each subregion, the following goal should be achieved:

$$\mathrm{Min}\left(\mathrm{Max}\left[d\left(p, s_k^i\right)\right]\right). \tag{36}$$

Without loss of generality, assume that there are u sensors in subregion R_i^{sub}. The goal was given by (36), which can be achieved by equally partitioning subregion R_i^{sub} into u grid $g_{i,j}$, $1 \le j \le u$. Let $c_{i,j}$ denote the center point of the grid $g_{i,j}$. These center points will be the new locations of u sensors in subregion R_i^{sub}.

The following gives an example to illustrate the data quality judgment of the grid $g_{i,1}$. As shown in Fig. 8, assume that there are three sensors in the subregion R_i^{sub}. The subregion R_i^{sub} is divided into three grids $g_{i,1}$, $g_{i,2}$, and $g_{i,3}$, with equal size. Let $c_{i,1}$, $c_{i,2}$, and $c_{i,3}$ denote the center points of grids $g_{i,1}$, $g_{i,2}$, and $g_{i,3}$, respectively. Let $\wp$ denote the number of edges of the grid $g_{i,1}$. The vertices of the grid $g_{i,1}$ are denoted by $p_{i,z}^1$ $(1 \le z \le \wp)$. Let $d_{i,z}^1$ $(1 \le z \le \wp)$ denote the distance from $c_{i,1}$ to $p_{i,z}^1$. Let $d_{\text{avg}}^{i,1}$ denote the average value of the distance difference between $d_{i,z}^1$ and $d_{i,h}^1$ $(1 \le h \le \wp)$. The value of

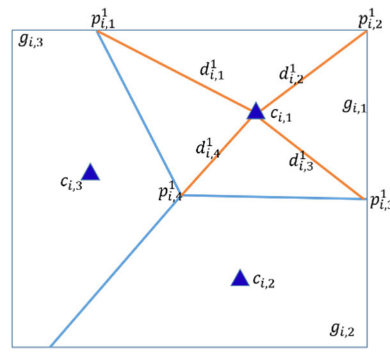

Fig. 8. Data quality judgment of grid g_{i1}.

$d_{\text{avg}}^{i,1}$ is calculated by applying (37). A smaller value of $d_{\text{avg}}^{i,1}$ indicates the higher data quality of the grid $g_{i,1}$

$$d_{\text{avg}}^{i,1} = \frac{\sum_{z=1}^{\wp}\sum_{z\neq h,h=1}^{\wp}\left(d_{i,z}^1 - d_{i,h}^1\right)^2}{\wp}. \tag{37}$$

The sensor that has the lowest energy consumption rate will move to the grid $g_{i,j}$, which has the lowest data quality. This expects to maximize the worst data quality of the grid $g_{i,j}$.

Until now, the mobile charger has finished its first round of recharging all sensors. Many parameters could be determined during the first round. Therefore, each sensor can regularly estimate its total working time, sensing frequency, as well as departure time in the second round.

It is noticed that sensor s_k^i needs to reserve the energy for moving to and back from the recharging station. Let $T_k^{\text{back},i}$ and $E_k^{\text{back},i}$ denote the time and the energy required for the sensor $s_k^i \in S_i$ moving from the recharging station RS_i to the relocated location $l_k^{\text{new},i}$, respectively. The values of $T_k^{\text{back},i}$ and $E_k^{\text{back},i}$ are calculated by applying the following equation:

$$T_k^{\text{back},i} = \frac{d\left(\mathrm{RS}_i, l_k^{\text{new},i}\right)}{vs} \tag{38}$$

$$E_k^{\text{back},i} = T_k^{\text{back},i} \times e_s^{\text{move\_disch}}. \tag{39}$$

Let $E_k^{\text{new\_rem},i}$ denote the total energy reserved by the sensor s_k^i for executing the sensing task at the location $l_k^{\text{new},i}$. The value of $E_k^{\text{new\_rem},i}$ can be calculated by the following equation:

$$E_k^{\text{new\_rem},i} = E_{\text{sensor}} - 2E_k^{\text{back},i}. \tag{40}$$

Let $T_i^{\text{new\_start\_recharge}}$ denote the second start recharging time of R_i^{sub}. Let $T_k^{\text{new\_departure},i}$ denote the departure time for recharging of sensor s_k^i at location $l_k^{\text{new},i}$. The value of $T_k^{\text{new\_departure},i}$ can be obtained by applying the following equation:

$$T_k^{\text{new\_departure},i} = T_i^{\text{new\_start\_recharge}} - T_k^{\text{back},i}. \tag{41}$$

Let $T_k^{\text{new\_work},i}$ denote the total working time for the sensor s_k^i at location $l_k^{\text{new},i}$. The value of $T_k^{\text{new\_work},i}$ can be calculated by the following equation:

$$T_k^{\text{new\_work},i} = T_k^{\text{new\_departure},i} - \left(T_i^{\text{start\_recharge}} + T_i^{\text{ch}} + T_k^{\text{back},i}\right). \tag{42}$$

Let $e_k^{\text{new\_sensing},i}$ denote the energy consumption rate of the sensor s_k^i for each sensing operation performed at the location $l_k^{\text{new},i}$. The value of $e_k^{\text{new\_sensing},i}$ is calculated by applying the following equation:

$$e_k^{\text{new\_sensing},i} = e_k^{\text{work\_disch},i} \Big/ f_k^{\text{best},i}. \tag{43}$$

Let $\psi_k^{\text{new},i}$ denote the number of sensing operations of the sensor s_k^i after returning to the new location. Therefore, the value of $\psi_k^{\text{new},i}$ can be calculated by applying the following equation:

$$\psi_k^{\text{new},i} = \frac{E_k^{\text{new\_rem},i}}{e_k^{\text{new\_sensing},i}}. \tag{44}$$

Let $f_k^{\text{new\_best},i}$ denote the best sensing frequency of s_k^i at location $l_k^{\text{new},i}$. The value of $f_k^{\text{new\_best},i}$ can be obtained by applying the following equation:

$$f_k^{\text{new\_best},i} = \psi_k^{\text{new},i} \Big/ T_k^{\text{new\_work},i}. \tag{45}$$

The following summarizes the proposed algorithm, as shown in Fig. 9.

Inputs: The unique ID, $l_k^{old,1}$, v_s, E_{sensor}, e_M^{char}, $e_s^{move\_disch}$, and $e_k^{work\_disch}$ of sensor $s_k^1 \in S_1$.

Output: the starting recharge time $T_i^{new\_start\_recharge}$ of sub-region R_i^{sub}, the departure time for recharging $T_k^{new\_departure,i}$, the total working time $T_k^{working,i}$, the best sensing frequency $f_k^{new\_best,i}$ of sensor s_k^i at location $l_k^{new,i}$.

/* Initial Phase */
Evaluate the number of sub-regions according to Exps. (15) - (18);
Calculate the starting recharge time points of all sub-regions according to Exps. (19) - (25);
Broadcast the starting recharge time points to all sensors in R;
/* Working Phase of the first round*/
Calculate working time based on the starting recharge time point according to Exps. (26) - (30);
Calculate the best sensing frequency $f_k^{best,i}$ of the $s_k^i \in S_i$ according to Exps. (33) - (35);
/* Recharging Phase*/
The mobile charger recharges all sensors in each sub-region;
/* The sensor that has the lowest energy consumption rate will move to the grid which has the lowest data quality */
If ($s_k^i = arg \min_{s_j^i \in R_i^{sub}} e_j^{work\_disch,i}$){
Apply Exp. (37) for calculating $d_{avg}^{i,j}$;
$g_{i,x} = arg \max_{g_{i,j} \in R_i^{sub}} d_{avg}^{i,j}$;
Let s_k^i move to the center point of the grid $g_{i,x}$; }
/* Many parameters could be determined during the first round. Therefore, each sensor can regularly estimate its total working time, sensing frequency as well as departure time in the second round. */
/* Working Phase of the second round*/
Calculate the departure time for recharging of sensor s_k^i at location $l_k^{new,i}$ according to Exps. (38) - (41);
Calculate the total working time for the sensor s_k^i at location $l_k^{new,i}$ according to Exp. (42);
Calculate the best sensing frequency of s_k^i at location $l_k^{new,i}$ according to Exps. (43) - (45).

Fig. 9. Pseudocode of the proposed algorithm.

V. Performance Evaluation

This section evaluates the performance improvement of the proposed algorithm against the existing recharging algorithms the minimum dead time (MDT) [21] and coverage-aware energy replenishment mechanism (CAERM) [22]. In the experiments, the three algorithms are compared in terms of data quality and stability. The following first presents the simulation model. Then, the simulation results are discussed.

A. Simulation Environment

The simulation parameters are given in Table IV. As shown in Fig. 10, the size of the monitoring region is 800 × 800 m. To evaluate the performance of this study, there are 200–1000 sensors randomly deployed in the monitoring area. The charging rate and the energy consumption for the movement of the mobile charger are set at 2 J/s and 0.3 J/m, respectively. The speed of the mobile charger is 1 m/s. The sensing radius is a constant value, which is ranging from 5 to 25 m. Since all sensors are mobile, the battery capacity of each sensor is set at 121 kJ, which is larger than that of the static sensor. The speed of each mobile sensor is set at a constant value of 0.3 m/s and the energy consumption for moving one unit distance is 0.1 J/m. The energy consumption rates of different sensors for working are different, ranging from 0.005 to 0.05 J/s. The sensing frequencies of different sensors are different, which are set at a value ranging from 0.1 to 20 times/h. The loss rates of data quality per unit of time and per unit distance are 0.1 and 0.3, respectively. The recharging distance of the mobile charger is 5 m.

B. Simulation Results

Fig. 11 investigates the spatial data quality by randomly selecting six locations in the monitoring area. From left top

TABLE IV
SIMULATION SETTINGS

Parameters	Values
Simulator	Matlab
Monitoring region	800 $m \times 800$ m
Deployment	Randomly
e_M^{char}	2J/s
$e_M^{move\_disch}$	0.3J/m
v_M	1m/s
r_s	5m – 25m
E_{sensor}	121KJ
v_s	0.3m/s
$e_s^{move\_disch}$	0.1J/m
$e_k^{work\_disch}$	0.005J/s - 0.05J/s
f_k	0.1-20 times/h
σ	0.1
ε	0.3
D_M	5m

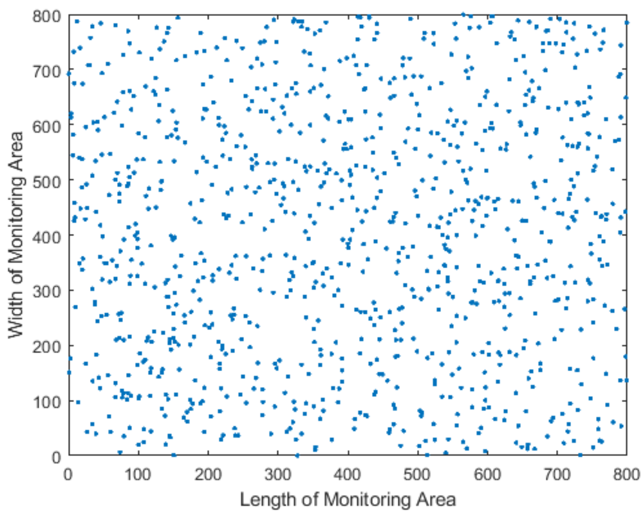

Fig. 10. Scenario where sensors are randomly deployed in the monitoring area.

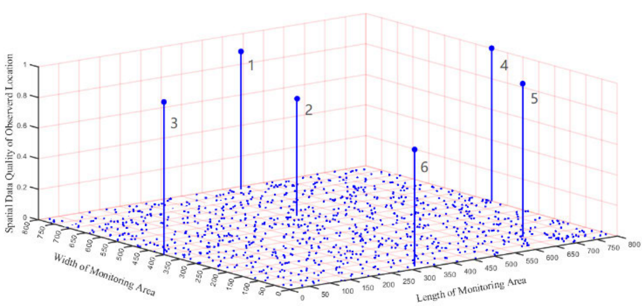

Fig. 11. Spatial data quality of randomly selecting six locations by applying the proposed algorithm.

to right bottom, the locations are marked with labels 1–6. As previously mentioned, the monitoring area is divided into m^2 equal-sized subregions. In general, there is a trend that the *spatial-DQ* is increased with the number of sensors in each subregion. For example, the locations with labels 3–5 have higher *spatial-DQ* because their densities are larger than the other three locations.

Fig. 12 further examines the effectiveness of each phase designed in the proposed recharging mechanism. The proposed algorithm consists of three phases: IN Phase, WR Phase, and RC Phase. The algorithm that applies the IN Phase and WR Phase is called P1P2. Similarly, P1P3 denotes the algorithm, which only applies the IN Phase and RC Phase, while P2P3 denotes the algorithm, which only applies the WR Phase and RC Phase. The value of the notation T_M is set at a half year. The elapsed time is ranging from one year to three years. As shown in Fig. 12, the proposed algorithm outperforms P1P2, P1P3, and P2P3 in terms of both *spatial* and *temporal* data qualities. This occurs because each phase contributes to the improvement of data quality. The IN Phase determines the locations and the number of recharging stations and calculates the starting recharge time of each subregion, which aims to improve the recharging efficiency and the *temporal-DQ* of the monitoring area. The WR Phase further calculates the working time and sensing frequency of each sensor, aiming to achieve maximal *temporal-DQ*. In the RC Phase, sensors are recharged and distributed to the appropriate locations to maintain the perpetual lifetime of sensors and maximize the *spatial-DQ*.

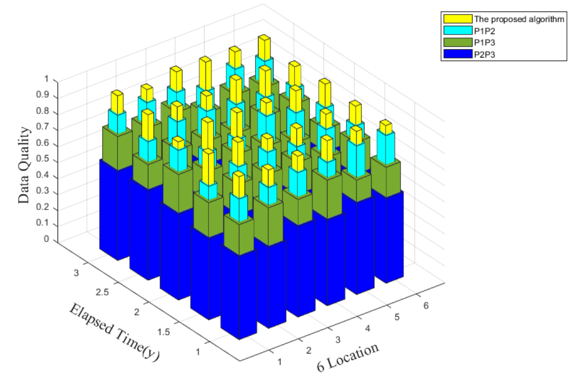

Fig. 12. Data quality comparison of six selected locations by applying the proposed algorithm, P1P2, P1P3, and P2P3 algorithms.

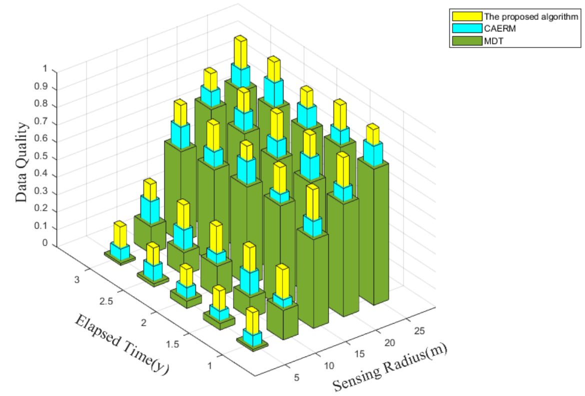

Fig. 13. Performance comparison of the proposed algorithm, CAERM, and MDT in terms of data quality by considering different sensing radii and elapsed time.

Fig. 13 further compares the data quality of three compared algorithms. The sensing radius varies from 5 to 25 m. The elapsed time is controlled ranging from one year to three years. There is a common trend that the data quality significantly increases with sensing radius. This occurs because the larger sensing radius leads to the larger *spatial-DQ*, increasing the total data quality. In comparison, the proposed algorithm outperforms the other two compared algorithms. This occurs

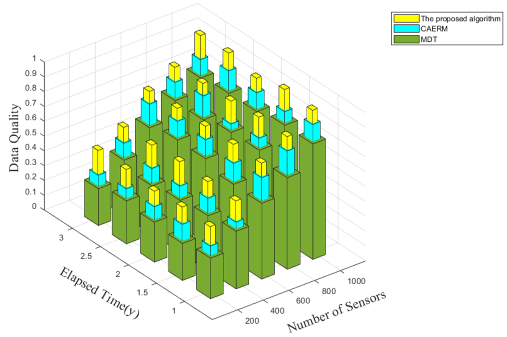

Fig. 14. Performance comparison of the proposed algorithm, CAERM, and MDT in terms of data quality by deploying the different number of sensors and varying elapsed time.

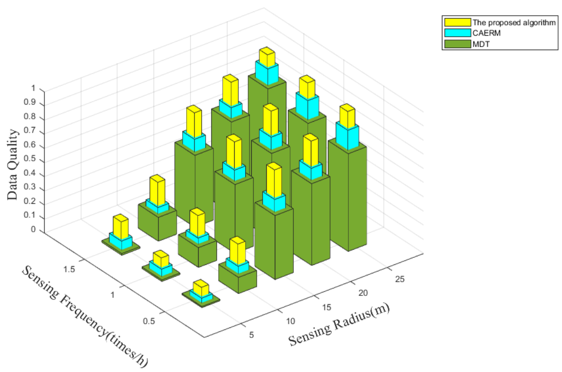

Fig. 15. Performance comparison of the proposed algorithm, CAERM, and MDT in terms of data quality by considering different sensing radii and frequencies.

because the proposed algorithm considers both the *temporal-DQ* and *spatial- DQ* when deciding on a recharging schedule. However, the compared CAERM only considered the coverages of sensors. The coverage consideration can only improve the *spatial- DQ*, without the consideration of *temporal DQ*. On the other hand, the compared MDT only considered the importance of different sensors and the bottleneck sensors in terms of remaining energy, without considering the *spatial* and *temporal* data qualities.

Fig. 14 aims to measure the data quality of three compared algorithms by deploying the different number of sensors and varying elapsed time. The number of sensors is ranging from 200 to 1000, while the elapsed time varies from one year to three years. As shown in Fig. 14, the data qualities of the three compared algorithms are generally increased with the number of sensors. This occurs because the densities of sensors will be increased with the number of deployed sensors. In comparison, the proposed algorithm outperforms the other two compared algorithms in all cases. This occurs because the proposed algorithm prioritizes recharging those sensors that have the larger contribution to the data quality.

Fig. 15 compares the data quality of the proposed algorithm, CAERM, and MDT under different sensing frequencies and different sensing radii. The sensing frequency varies from 0.5 to 1.5 times/h, while the sensing radius varies from 5 to 25 m. In Fig. 15, a common trend of the three algorithms is that the data quality is increased with both the sensing radius and sensing frequency. This occurs because the increase of the

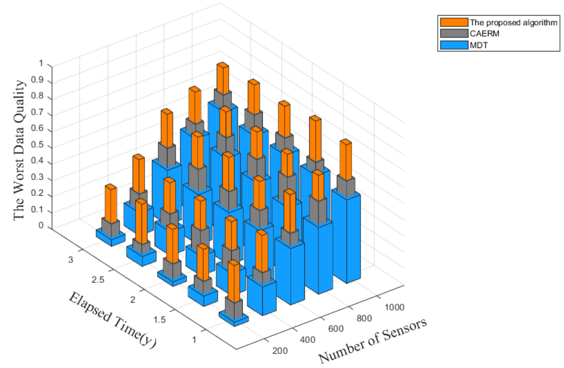

Fig. 16. Performance comparison of the proposed algorithm, CAERM, and MDT in terms of the worst data quality by considering different sensing radii and elapsed time.

sensing frequency can lead to better temporal-DQ, while the increase of sensing radius further increases the spatial-DQ.

Fig. 16 further compares the three algorithms in terms of the worst data quality by considering different sensing radii and elapsed time. A common trend of the three algorithms is that the worst data qualities are increased with the sensing radius. This occurs because a larger sensing radius can improve the *spatial-DQ* and hence increase the total data quality. In comparison, the proposed algorithm outperforms the other CREAM and MDT algorithms. This occurs because the RC Phase of the proposed algorithm considers the weakest data quality. After finishing the recharging task, some sensors, which consume the least working energy, will move to the location having the weakest data quality. However, the existing CREAM and MDT did not consider the weakest data quality when deciding on the recharging schedule.

Fig. 17 compares the MCEI of the three compared algorithms. The battery capacity of each sensor varies from 1 K to 4 kJ, while the number of sensors varies from 200 to 1000. The MCEI is defined as the total energy of sensors obtained from the mobile charger divided by the distance moved by the mobile charger, as shown in (46). In case the mobile charger travels a short path and also recharges more sensors at one time, the MCEI is high. On the contrary, if the mobile charger travels a long path or recharges a few sensors at one time, the MCEI is low. The MCEI formula is given as follows:

$$\mathrm{MCEI} = \frac{n \times E_{\text{sensor}}}{\sum_{i=1}^{m^2} d(\mathrm{MC}, \mathrm{RS}_i)}. \tag{46}$$

As shown in Fig. 17, the proposed algorithm yields the largest MCEI value because the mobile charger will arrive at each recharging station and recharge all sensors waiting at that station. This can maximize the MCEI since many sensors can be recharged simultaneously. In the existing CREAM, the mobile charger recharges one sensor at a time. Therefore, the mobile charger paid a certain movement cost for recharging each sensor. In the existing MDT algorithm, the mobile charger recharged one sensor at a time if the sensor was closer to the sink node. This also raises a certain distance cost for recharging each sensor.

Fig. 18 studies the fairness index of the compared three algorithms. The number of sensors is ranging

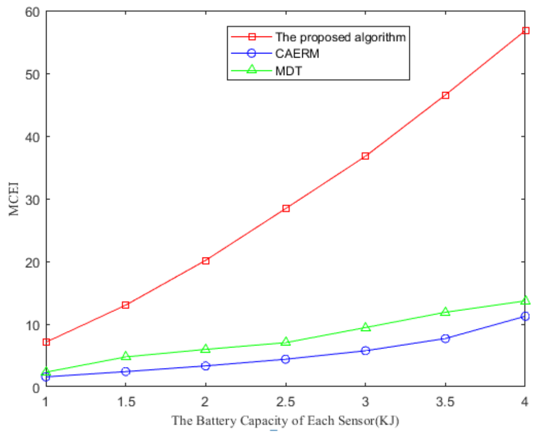

Fig. 17. Performance comparison of the proposed algorithm, CAERM, and MDT in terms of efficiency of MC by (a) battery capacity of each sensor and deploying the different (b) number of sensors.

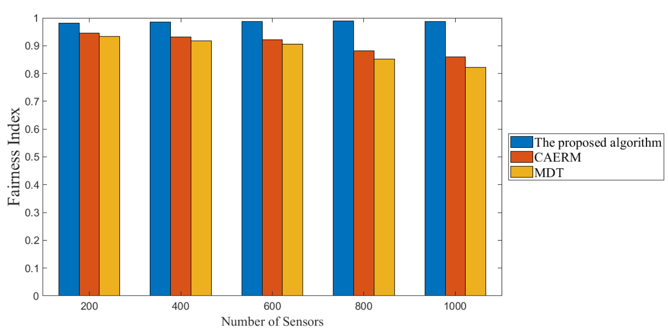

Fig. 18. Performance comparison of the proposed algorithm, CAERM, and MDT in terms of fairness index by deploying the different number of sensors.

from 200 to 1000. Let ξ_{fairness} denote the *Fairness Index* of data quality of the monitoring area. Let q_i denote data quality of the ith space point p_i, $1 \leq i \leq \rho$. The following equation calculates the value of ξ_{fairness}:

$$\xi_{\text{fairness}} = \frac{\left(\sum_{i=1}^{m\rho} q_i\right)^2}{\rho \sum_{i=1}^{\rho} q_i^2}. \tag{47}$$

As shown in Fig. 18, the fairness index of the proposed algorithm almost achieves 0.98 in all cases. It indicates that the data quality of the monitoring area is stable. In addition, the proposed algorithm outperforms the existing CAERM and MDT algorithms in terms of fairness index. This occurs because the proposed algorithm considers the worst data quality and allocates some sensors with the lowest energy consumption to the location with the worst data quality.

VI. Conclusion

This article proposes the recharging algorithm for MWRSNs, aiming to sustain the lifetime of sensors and maximize the *spatial* and *temporal* data quality. The mobility of the sensors can help reduce the path costs of the mobile charger. Besides, the proposed recharging algorithm considers not only the recharging efficiency but also the data quality. The proposed algorithm mainly consists of three phases. In the IN Phase, the monitoring area is divided into several subregions and the virtual recharging center of each subregion is set up. Then, the mobile charger determines the starting recharging time of each subregion. The sensors of each subregion automatically move to the virtual recharging center for recharging, aiming to reduce the traveling path length of the mobile charger. In the WR Phase, each sensor further calculates the working time according to the starting recharging time and modulates the sensing frequency, aiming to improve the *temporal-DQ*. In RC Phase, the sensors are recharged by the mobile charger. To maximize the *spatial-DQ* and improve the worst data quality, the sensor that has the lowest energy consumption is scheduled to monitor the lowest monitoring quality area. The performance study demonstrates that the proposed algorithm outperforms the other existing studies in terms of recharging effectiveness and DQ.

References

[1] Z. Cui et al., "A hybrid BlockChain-based identity authentication scheme for multi-WSN," *IEEE Trans. Services Comput.*, vol. 13, no. 2, pp. 241–251, Mar. 2020.

[2] J. Uthayakumar, M. Elhoseny, and K. Shankar, "Highly reliable and low-complexity image compression scheme using neighborhood correlation sequence algorithm in WSN," *IEEE Trans. Rel.*, vol. 69, no. 4, pp. 1398–1423, Dec. 2020.

[3] B. Li, Y. Zou, J. Zhu, and W. Cao, "Impact of hardware impairment and co-channel interference on security-reliability trade-off for wireless sensor networks," *IEEE Trans. Wireless Commun.*, vol. 20, no. 11, pp. 7011–7025, Nov. 2021.

[4] S. Chamanian, S. Baghaee, H. Ulusan, Ö. Zorlu, E. Uysal-Biyikoglu, and H. Külah, "Implementation of energy-neutral operation on vibration energy harvesting WSN," *IEEE Sensors J.*, vol. 19, no. 8, pp. 3092–3099, Apr. 2019.

[5] S. S. Desai and M. J. Nene, "Multihop trust evaluation using memory integrity in wireless sensor networks," *IEEE Trans. Inf. Forensics Security*, vol. 16, pp. 4092–4100, 2021.

[6] A. Naeem, A. R. Javed, M. Rizwan, S. Abbas, J. C. Lin, and T. R. Gadekallu, "DARE-SEP: A hybrid approach of distance aware residual energy-efficient SEP for WSN," *IEEE Trans. Green Commun. Netw.*, vol. 5, no. 2, pp. 611–621, Jun. 2021.

[7] J. Hu, J. Luo, Y. Zheng, and K. Li, "Graphene-grid deployment in energy harvesting cooperative wireless sensor networks for green IoT," *IEEE Trans. Ind. Informat.*, vol. 15, no. 3, pp. 1820–1829, Mar. 2019.

[8] Y. Xiong, G. Chen, M. Lu, X. Wan, M. Wu, and J. She, "A two-phase lifetime-enhancing method for hybrid energy-harvesting wireless sensor network," *IEEE Sensors J.*, vol. 20, no. 4, pp. 1934–1946, Feb. 2020.

[9] F. Deng, X. Yue, X. Fan, S. Guan, Y. Xu, and J. Chen, "Multisource energy harvesting system for a wireless sensor network node in the field environment," *IEEE Internet Things J.*, vol. 6, no. 1, pp. 918–927, Feb. 2019.

[10] A. Boukerche, Q. Wu, and P. Sun, "A novel two-mode QoS-aware mobile charger scheduling method for achieving sustainable wireless sensor networks," *IEEE Trans. Sustain. Comput.*, vol. 7, no. 1, pp. 14–26, Jan. 2022.

[11] W. Ouyang et al., "Utility-aware charging scheduling for multiple mobile chargers in large-scale wireless rechargeable sensor networks," *IEEE Trans. Sustain. Comput.*, vol. 6, no. 4, pp. 679–690, Oct. 2021.
[12] Z. Sheng, C. Mahapatra, V. C. M. Leung, M. Chen, and P. K. Sahu, "Energy efficient cooperative computing in mobile wireless sensor networks," *IEEE Trans. Cloud Comput.*, vol. 6, no. 1, pp. 114–126, Jan. 2018.
[13] S. Salari, I.-M. Kim, and F. Chan, "Distributed cooperative localization for mobile wireless sensor networks," *IEEE Wireless Commun. Lett.*, vol. 7, no. 1, pp. 18–21, Feb. 2018.
[14] N.-T. Nguyen and B.-H. Liu, "The mobile sensor deployment problem and the target coverage problem in mobile wireless sensor networks are NP-hard," *IEEE Syst. J.*, vol. 13, no. 2, pp. 1312–1315, Jun. 2019.
[15] W. Xu, W. Liang, X. Jia, Z. Xu, Z. Li, and Y. Liu, "Maximizing sensor lifetime with the minimal service cost of a mobile charger in wireless sensor networks," *IEEE Trans. Mobile Comput.*, vol. 17, no. 11, pp. 2564–2577, Nov. 2018.
[16] Y. Shu et al., "Near-optimal velocity control for mobile charging in wireless rechargeable sensor networks," *IEEE Trans. Mobile Comput.*, vol. 15, no. 7, pp. 1699–1713, Jul. 2016.
[17] L. Fu, L. He, P. Cheng, Y. Gu, J. Pan, and J. Chen, "ESync: Energy synchronized mobile charging in rechargeable wireless sensor networks," *IEEE Trans. Veh. Technol.*, vol. 65, no. 9, pp. 7415–7431, Sep. 2016.
[18] G. Han, H. Guan, J. Wu, S. Chan, L. Shu, and W. Zhang, "An uneven cluster-based mobile charging algorithm for wireless rechargeable sensor networks," *IEEE Syst. J.*, vol. 13, no. 4, pp. 3747–3758, Dec. 2019.
[19] M. Tian, W. Jiao, J. Liu, and S. Ma, "A charging algorithm for the wireless rechargeable sensor network with imperfect charging channel and finite energy storage," *Sensors*, vol. 19, no. 18, pp. 3887–3905, Sep. 2019.
[20] T. Chen, J. Chen, X. Gao, and T. Chen, "Mobile charging strategy for wireless rechargeable sensor networks," *Sensors*, vol. 22, pp. 359–382, Jan. 2022.
[21] M. Tian, W. Jiao, and J. Liu, "The charging strategy of mobile charging vehicles in wireless rechargeable sensor networks with heterogeneous sensors," *IEEE Access*, vol. 8, pp. 73096–73110, 2020.
[22] H. Yu, C.-Y. Chang, Y. Wang, D. S. Roy, and X. Bai, "CAERM: Coverage aware energy replenishment mechanism using mobile charger in wireless sensor networks," *IEEE Sensors J.*, vol. 21, no. 20, pp. 23682–23697, Oct. 2021.
[23] M. Angurala, M. Bala, and S. S. Bamber, "Implementing MRCRLB technique on modulation schemes in wireless rechargeable sensor networks," *Egyptian Informat. J.*, vol. 22, no. 4, pp. 473–478, Dec. 2021.
[24] M. Angurala et al., "Testing solar-MAODV energy efficient model on various modulation techniques in wireless sensor and optical networks," *Wireless Netw.*, vol. 28, pp. 413–425, Jan. 2022.
[25] X. Li, L. Zheng, Z. Wang, C. Chen, W. Wang, and Y. Hu, "Multi-node energy policy for wireless sensor networks," in *Proc. IEEE Int. Conf. Smart Internet Things (SmartIoT)*, Aug. 2018, pp. 58–63.

Zhijie Hu received the M.S. degree in communication and information systems from Xi'an Technological University, Xi'an, China, in 2011. She is currently pursuing the Ph.D. degree in computer science and technology with Xi'an Jiaotong University, Xi'an.

She is currently a Lecturer with the School of Information Engineering, Xi'an Eurasia University, Xi'an. Her research interests include the Internet of Things, wireless sensor networks, and artificial intelligence.

Chih-Yung Chang (Member, IEEE) received the Ph.D. degree in computer science and information engineering from National Central University, Taoyuan, Taiwan, in 1995.

He is currently a Distinguish Professor with the Department of Computer Science and Information Engineering, Tamkang University, New Taipei, Taiwan. His current research interests include artificial intelligence, the Internet of Things, wireless sensor networks, and smart healthcare.

Dr. Chang has served as an Associate Guest Editor for several SCI-indexed journals, including *International Journal of Ad Hoc and Ubiquitous Computing* (IJAHUC) from 2011 to 2021, *International Journal of Distributed Sensor Networks* (IJDSN) from 2012 to 2014, *IET Communications* in 2011, *Telecommunication Systems* (TS) in 2010, *Journal of Information Science and Engineering* (JISE) in 2008, and *Journal of Internet Technology* (JIT) from 2004 to 2008.

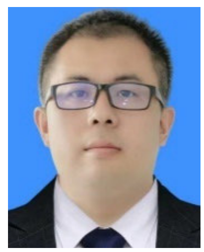

Ruibing Shen received the M.S. degree in control theory and control engineering from Xi'an Technological University, Xi'an, China, in 2011.

He is currently an Associate Professor with the School of Information Engineering, Xi'an Eurasia University, Xi'an. His research interests include automatic control and intelligent hardware.

Chin-Hwa Kuo received the B.S. degree in mechanical engineering from Chung-Yuan University, Taoyuan, Taiwan, in 1980, the M.S. degree in electrical engineering from Marquette University, Milwaukee, WI, USA, in 1989, and the Ph.D. degree in electrical engineering from the University of Notre Dame, South Bend, IN, USA, in 1994.

Currently, he is a Full Professor with the Department of Computer Science and Information Engineering, Tamkang University, Taipei, Taiwan, where he is also the Chief of Information Officer. His research interests include multimedia processing and applications, learning analytics, and large-scale deployment of information and communications technology (ICT) in education.

Diptendu Sinha Roy received the Ph.D. degree in engineering from the Birla Institute of Technology, Mesra, Ranchi, India, in 2010.

In 2016, he joined the Department of Computer Science and Engineering, National Institute of Technology (NIT) Meghalaya, Shillong, India, as an Associate Professor, where he has been the Chair of the Department of Computer Science and Engineering since January 2017. Prior to his stint with NIT Meghalaya, he had served with the Department of Computer Science and Engineering, National Institute of Science and Technology, Berhampur, India. His current research interests include software reliability, distributed and cloud computing, and the IoT, specifically applications of artificial intelligence/machine learning for smart integrated systems.

Dr. Roy is a member of the IEEE Computer Society.